The Origin of High-velocity Stars from *Gaia* and LAMOST

Cuihua Du[1] , Hefan Li[2] , Heidi Jo Newberg[3] , Yuqin Chen[1,4] , Jianrong Shi[1,4] , Zhenyu Wu[1,4] , and Jun Ma[1,4]

[1] College of Astronomy and Space Sciences, University of Chinese Academy of Sciences, Beijing 100049, People's Republic of China; ducuihua@ucas.ac.cn
[2] School of Physical Sciences, University of Chinese Academy of Sciences, Beijing 100049, People's Republic of China
[3] Department of Physics, Applied Physics and Astronomy, Rensselaer Polytechnic Institute, Troy, NY 12180, USA; newbeh@rpi.edu
[4] Key Laboratory of Optical Astronomy, National Astronomical Observatories, Chinese Academy of Sciences, Beijing 100012, People's Republic of China

Abstract

Based on the second *Gaia* data release and spectroscopy from the Large Sky Area Multi-object Fiber Spectroscopic Telescope (LAMOST) Data Release 5, we define the high-velocity (HiVel) stars sample as those stars with $v_{gc} > 0.85v_{esc}$, and derived the final sample of 24 HiVel stars with stellar astrometric parameters and radial velocities. Most of the HiVel stars are metal poor and α-enhanced. In order to further explore the origin of these HiVel stars, we traced the backward orbits of each HiVel star in the Galactic potential to derive probability parameters that are used to classify these HiVel stars. Of these, 5 stars are from the tidal debris of disrupted dwarf galaxy, and 19 stars are runaway-star candidates originating from the stellar disk.

1. Introduction

High-velocity (HiVel) stars move fast enough that they can escape the gravitational potential of the Galaxy. With the development of large spectroscopic surveys such as the Sloan Digital Sky Survey (SDSS), the RAdial Velocity Experiment (RAVE), the Large Sky Area Multi-object Fiber Spectroscopic Telescope (LAMOST), and *Gaia*, a large number of high-velocity candidates have been reported (e.g., Brown et al. 2006, 2009, 2012, 2014; Li et al. 2012, 2018; Zheng et al. 2014; Zhong et al. 2014; Geier et al. 2015; Zhang et al. 2016; Huang et al. 2017; Bromley et al. 2018; Du et al. 2018; Marchetti et al. 2018). HiVel stars are intriguing because they not only flag the presence of extreme dynamical and astrophysics processes, but they also can be used as dynamical traces of integral properties of the Galaxy. In particular, the origin of HiVel stars can provide useful information about the environments from which they are produced. In general, there are three subclasses for HiVel stars, and they have different origins. First of all, the fastest stars in our Galaxy are hypervelocity stars (HVSs), which have extreme velocities above the escape speed of the Milky Way. HVSs can obtain their large velocity from a number of different processes. Hills (1988) first theoretically predicted the formation of HVSs via three-body interactions between a binary star system and the massive black hole (MBH) in the Galactic Center (GC). Other possible alternative mechanisms include the interaction between single stars and a hypothetical binary MBH (Yu & Tremaine 2003; Merritt 2006; Sesana et al. 2006, 2007), and the interaction between a globular cluster with a single or a binary MBH in the GC (e.g., Capuzzo-Dolcetta & Fragione 2015; Fragione & Capuzzo-Dolcetta 2016). Since the first HVS was discovered by Brown et al. (2005), almost two dozen unbound HVSs of late B-type with masses between 2.5 and 4 $M_{\odot}$ (Brown et al. 2014; Zheng et al. 2014; Geier et al. 2015; Huang et al. 2017) have been found from systematic searches. In addition to the unbound population of HVSs, all mechanisms mentioned above also predicted a population of bound HVSs (Bromley et al. 2009). For example, Brown et al. (2014) identified 16 such stars whose Galactic rest-frame velocities exceed 275 km s^{-1}.

"Runaway stars" are another subclass of high-velocity stars and were first introduced as O- and B-type stars by Blaauw (1961).

Runaway stars are thought to have formed in the disk and then were ejected into the halo. These stars can provide an important connection between star formation in the Galactic disk and halo. In general, runaway stars can be produced through two main formation mechanisms: (1) supernova explosions in stellar binary systems (e.g., Blaauw 1961; Portegies 2000; Gvaramadze et al. 2009; Wang et al. 2013), and (2) dynamical encounters due to multi-body encounters in dense stellar systems (e.g., Bromley et al. 2009; Gvaramadze et al. 2009). Both mechanisms can produce both low- and high-mass runaway stars. But the majority of runaway stars in the literature are high-mass O- and B-type stars with ejection velocities less than 200 km s^{-1} (Perets & Šubr 2012). Recent results show that it is possible for low-mass G-/K-type stars with ejection velocities up to ~1300 km s^{-1} (Tauris 2015). In addition to the two classes of HiVel stars mentioned above, there also exist fast halo stars from the tidal debris of an accreted and disrupted dwarf galaxy (Abadi et al. 2009; Teyssier et al. 2009).

In order to distinguish between these scenarios, recent studies have used chemical and kinematic information to determine the origin of HiVel stars (e.g., Li et al. 2012; Geier et al. 2015; Hawkins et al. 2015; Marchetti et al. 2018). For example, if HiVel stars are more metal rich ([Fe/H] > −0.5) than expected for the inner halo, and the [α/Fe] measurements are consistent with those of disk stars, it may suggest that these metal-rich HiVel stars formed in the disk and were subsequently dynamically ejected into the halo (Bromley et al. 2009; Purcell et al. 2010; Hawkins et al. 2015). The kinematic studies need to use accurate proper motions and parallaxes to calculate trajectories with sufficiently small uncertainties. The second *Gaia* data release (*Gaia* DR2; Gaia Collaboration et al. 2018) provides an unprecedented sample of precisely and accurately measured sources.

In this Letter, we use *Gaia* proper motions (Gaia Collaboration et al. 2016a, 2016b) and radial velocities combined with radial velocities and metallicities derived from LAMOST stellar spectra (Zhao et al. 2012) to study the origin of HiVel stars. In Section 2, we briefly describe the data and target selection. In Section 3, we identify these HiVel stars and explore their origin, including an analysis of the chemical

abundances and orbital properties. The conclusions and summary are given in Section 4.

2. Data and Target Selection

2.1. Data

Gaia DR2 includes high-precision measurements of nearly 1.7 billion stars (Gaia Collaboration et al. 2018). As well as positions, the data also include astrometry, photometry, radial velocities, and information on astrophysical parameters and variability, for sources brighter than magnitude 21. This data set contains parallaxes and mean proper motions for about 1.3 billion of the brightest stars. Radial velocity (RV) measurements rv_G for a subset of 7,224,631 stars with an effective temperature from 3550 to 6990 K are included in *Gaia* DR2; the typical uncertainties are a few hundreds of $m\,s^{-1}$ at the bright end of the *Gaia G* magnitude, and a few $km\,s^{-1}$ at the faint end. In the following we will focus on a subsample of stars.

LAMOST is a 4 m quasi-meridian reflective Schmidt telescope that is equipped with 4000 fibers within a field of view of 5°. The LAMOST spectrograph has a resolution of $R \sim 1800$ and wavelength range spanning 3700–9000 Å (Cui et al. 2012).The survey reaches a limiting magnitude of $r = 17.8$ (where r denotes magnitude in the SDSS r-band), but most targets are brighter than $r \sim 17$. The LAMOST Stellar Parameter Pipeline (Wu et al. 2011; Luo et al. 2015) estimates parameters, including RV, effective temperature, surface gravity, and metallicity ([Fe/H]) from LAMOST spectra. The accuracies in measuring RV (rv_L) and [Fe/H] at $R = 1800$ are expected to be $7\,km\,s^{-1}$ and 0.1 dex, respectively (Deng et al. 2012; Zhao et al. 2012). The LAMOST Stellar Parameter Pipeline at Peking University (LSP3; Xiang et al. 2015, 2017) gives α-element to iron abundance ratio [α/Fe]. In total, there are over 5 million stars in the A-, F-, G-, and K-type star catalog.

From the quasars and validation solutions, Lindegren et al. (2018) estimated that systematics in the parallaxes depending on position, magnitude, and color are generally below 0.1 mas, but the parallaxes are on the whole too small by about 0.029 mas. The radial velocity zero-points (RVZPs) of large-scale stellar spectroscopic surveys need to be determined and corrected for future studies. Huang et al. (2018) presented a new catalog of 18,080 RV standard stars selected from the APO Galactic Evolution Experiment (APOGEE) data. To determine the RVZP of LAMOST measurements, we cross-match the APOGEE RV standard stars with the LAMOST DR5 catalog and obtain 3580 common stars of LAMOST spectral signal-to-noise ratio (S/N) greater than 20. The stars yield a mean difference $\Delta rv = -4.70\,km\,s^{-1}$ and a standard deviation s.d. = $4.45\,km\,s^{-1}$. We also cross-match the APOGEE RV standard stars with *Gaia* DR2 and obtain 8786 common stars. The mean difference found by these stars is $\Delta rv = 0.47\,km\,s^{-1}$, with a standard deviation s.d. = $1.40\,km\,s^{-1}$. We calibrate the parallax and RV measurements with determined offsets in the following study.

2.2. HiVel Candidate Selection

Our initial sample was obtained by cross-matching between the *Gaia* and LAMOST catalogs based on stellar position. We first select those stars with S/N $\geqslant$ 20. In order to ensure the reliable RV, we also use the selection criterion $|rv_G - rv_L| \leqslant 10\,km\,s^{-1}$.
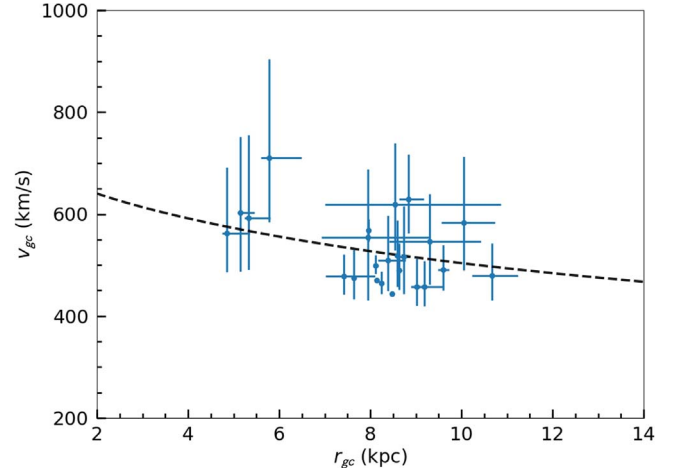
Figure 1. Total velocity in the Galactic rest frame v_{gc} as a function of Galactocentric distance r_{gc} for 24 HiVel stars. The black dashed line is the median escape speed from Williams et al. (2017) and the blue dots represent the HiVel stars sample.

We adopt the weighted means for RV and its error

$$rv = \frac{rv_G\,\sigma_L^2 + rv_L\,\sigma_G^2}{\sigma_G^2 + \sigma_L^2}, \quad \sigma_{rv}^2 = \frac{\sigma_L^2\,\sigma_G^2}{\sigma_G^2 + \sigma_L^2}$$

where G and L represent *Gaia* and LAMOST, respectively.

Adopting the method from Luri et al. (2018), we use Bayesian analysis to determine the distance and velocity of the stars. We adopt the exponentially decreasing space density prior in distance d (Bailer-Jones et al. 2018)

$$P(d \mid L) \propto d^2 \exp(-d/L)$$

and assume uniform priors on $v_{R.A.}$, $v_{decl.}$, v_r. So we can express the posterior distribution

$$P(\boldsymbol{\theta} \mid \boldsymbol{x}) \propto \exp\left[-\frac{1}{2}(\boldsymbol{x} - \boldsymbol{m}(\boldsymbol{\theta}))^T C_x^{-1}(\boldsymbol{x} - \boldsymbol{m}(\boldsymbol{\theta})) \right] P(d|L)$$

where $\boldsymbol{\theta} = (d, v_{R.A.}, v_{decl.}, v_r)^T$, $\boldsymbol{x} = (\varpi, \mu_{\alpha*}, \mu_\delta, rv)^T$, $\boldsymbol{m} = (1/d, v_{R.A.}/kd, v_{decl.}/kd, v_r)^T$, $k = 4.74$, and C_x^{-1} is the covariance matrix. The positions and velocities are derived from the most probable value of d, $v_{R.A.}$, $v_{decl.}$, v_r.

Total velocities in the Galactic rest frame are computed correcting radial velocities and proper motions for the solar and the local standard of rest (LSR) motion. Here, the distance of the Sun from the GC $R_\odot = 8.2$ kpc, and the Sun has an offset from the local disk $z_\odot = 25$ pc (Bland-Hawthorn & Gerhard 2016). We calculate each star's Galactic space-velocity components, U, V and W, from its tangential velocities, distance, and RV (Johnson & Soderblom 1987). We assume that the LSR velocity is $V_{LSR} = 232.8\,km\,s^{-1}$ in the direction of rotation (McMillan 2017) and the solar peculiar motion $(U, V, W) = (10., 11., 7.)\,km\,s^{-1}$ (Tian et al. 2015; Bland-Hawthorn & Gerhard 2016) relative to the LSR. The median escape speed v_{esc} can be derived from Williams et al. (2017). Applying the criteria mentioned above and further constraining the total velocity $v_{gc} > 0.85 v_{esc}$, we obtain 37 candidates of HiVel stars.

Then we use Markov Chain Monte Carlo (MCMC) sampler EMCEE to estimate error of these stars. We use 20 walkers and sample for 200 iterations. We run 1000 burn-in steps to let the walkers find the starting point. In order to filter out the
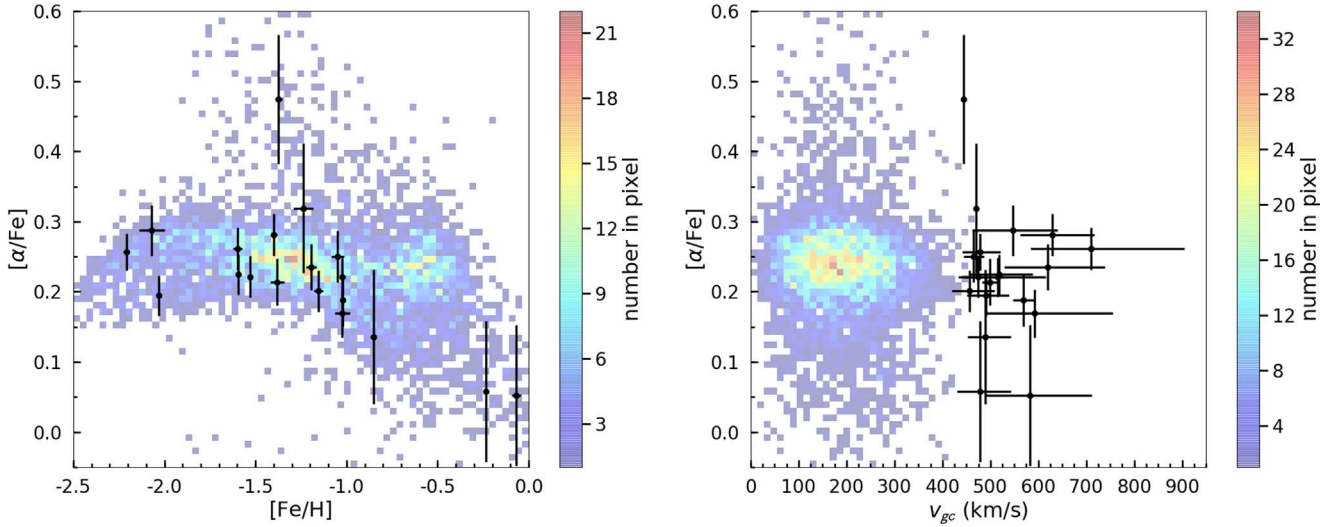
Figure 2. Left panel: chemical abundance distribution $[\alpha/\text{Fe}]$ vs. $[\text{Fe/H}]$ of 24 HiVel stars. Right panel: chemical abundance distribution $[\alpha/\text{Fe}]$ vs. v_{gc}. The black points represent the HiVel stars. The halo stars that selected by Toomre Diagram are shown as background for comparison and the color coding corresponds to the number of halo stars in each pixel.

uncertain candidates, we remove stars with $\sigma_{\text{vgc}}/v_{\text{gc}} < 0.3$ and $\sigma_{\text{rgc}} < 2$ kpc. Finally, we get a sample of 24 HiVel stars.

Figure 1 shows the total velocity in the Galactic rest frame v_{gc} as a function of Galactocentric distance r_{gc} for 24 HiVel stars. Most of our high-velocity stars lie in the inner region of the Galaxy. The catalog of 24 HiVel stars is given in Table 2 and Table 3 of the Appendix.

3. Chemical Abundances and Orbits of HiVel Stars

The distribution in $[\alpha/\text{Fe}]$ space also provides valuable information about the timescales and intensities of star formation in the populations involved. The study by Nissen & Schuster (2010) proposed that the high-α stars may have been born in the disk or bulge of the Milky Way and heated to halo kinematics by merging satellite galaxies, or else were simply members of the early generations of halo stars born during the collapse of a proto-Galactic gas cloud, while the low-α stars may have been accreted from dwarf galaxies. Therefore, the abundance space of $[\alpha/\text{Fe}]$ versus $[\text{Fe/H}]$ is particularly useful in tracing the origin of individual stars (Lee et al. 2015). Figure 2 shows the chemical abundance distribution $[\alpha/\text{Fe}]$ versus $[\text{Fe/H}]$ and $[\alpha/\text{Fe}]$ versus v_{gc} for some HiVel stars. For comparison, we also add the halo stars as background in the figure. The halo stars are defined as having $|v_{\text{gc}} - v_{\text{LSR}}| > 232.8$ km s^{-1}, where $v_{\text{LSR}} = (0, 232.8, 0)$ km s^{-1} in the Galactocentric Cartesian coordinates. We can see from Figure 2 that most of our HiVel stars are metal poor and slightly α enriched, with a mean α abundance of $\overline{[\alpha/\text{Fe}]} = +0.22$ dex, which is consistent with the result of Hawkins et al. (2015), with a mean α abundance of $\overline{[\alpha/\text{Fe}]} = +0.24$ dex. It shows some HiVel stars could have originated from the GC or disk, and some from dwarf galaxies. For example, GLHV-8 has high $[\text{Fe/H}] = -0.24$ and low $[\alpha/\text{Fe}] = 0.06$ that appears to be coming from a thick disk. The large dispersion in the $[\alpha/\text{Fe}]$ could result from the uncertainty of the individual $[\alpha/\text{Fe}]$ estimates. The large uncertainty in the $[\alpha/\text{Fe}]$ estimates is a result of the relatively low resolution of the LAMOST spectra. We are looking forward to high-resolution spectra of these stars in the future.

To better understand the ejection location of our HiVel stars, we study their orbital properties by adopting the Galaxy potential model provided in McMillan (2017). This model includes components that represent the contribution of the cold gas disks near the Galactic plane, as well as thin and thick stellar disks, a bulge component, and a dark-matter halo. For each star, we use 4000 MCMC realizations as discussed in Section 2.2. We integrate each orbit back in a total time of 2 Gyr, starting with the current position of each star. If a star reaches the maximum potential point Φ_{max} in 2 Gyr, we will call it unbound. The orbit will be cut off at that point to ensure its reliability, resulting in the probability of a star being unbound P_{ub}.

As an example, Figure 3 gives the derived backward orbits for three subclasses of HiVel stars, integrated back 2 Gyr. The red dot represents the present position, and the black dot represents the GC.

Adopting the method from Marchetti et al. (2018), we could derive the position of a star crossing the disk and calculate the distance from the GC to the crossing point. The minimum value of the distance is called $R_{\text{min,2 Gyr}}$. Some stars' velocities are slightly smaller than v_{esc}, therefore 2 Gyr may not be enough for them to cross the disk. In this case we increase the trace-back time to 5 Gyr and get the minimum crossing radius $R_{\text{min,5 Gyr}}$ just like above. Then we can get the probability P_{gc} that $R_{\text{min,2 Gyr}} < 1$ kpc and P_{MW} that $R_{\text{min,5 Gyr}} < 25$ kpc (Xu et al. 2015). They measure the probability that stars are derived from the GC and the classified criteria are shown in Table 1. Here, "HVS" represents the fastest stars in the Galaxy that are HiVel; "OUT" represents fast halo stars from the tidal debris of dwarf galaxy; "HRS" represents hyper-runaway-star candidates; and "RS" represents the runaway stars.

As seen in Figure 3, the left panels represent the "OUT" candidate that is from the tidal debris of dwarf galaxy, and the right panels represent runaway stars and hyper-runaway stars that are thought to have formed in the disk and ejected into the halo.

4. Conclusions and Summary

Using *Gaia* DR2 data combined with observations from the ground-based spectroscopic survey LAMOST DR5, we cross-matched the initial sample and defined our HiVel star sample as
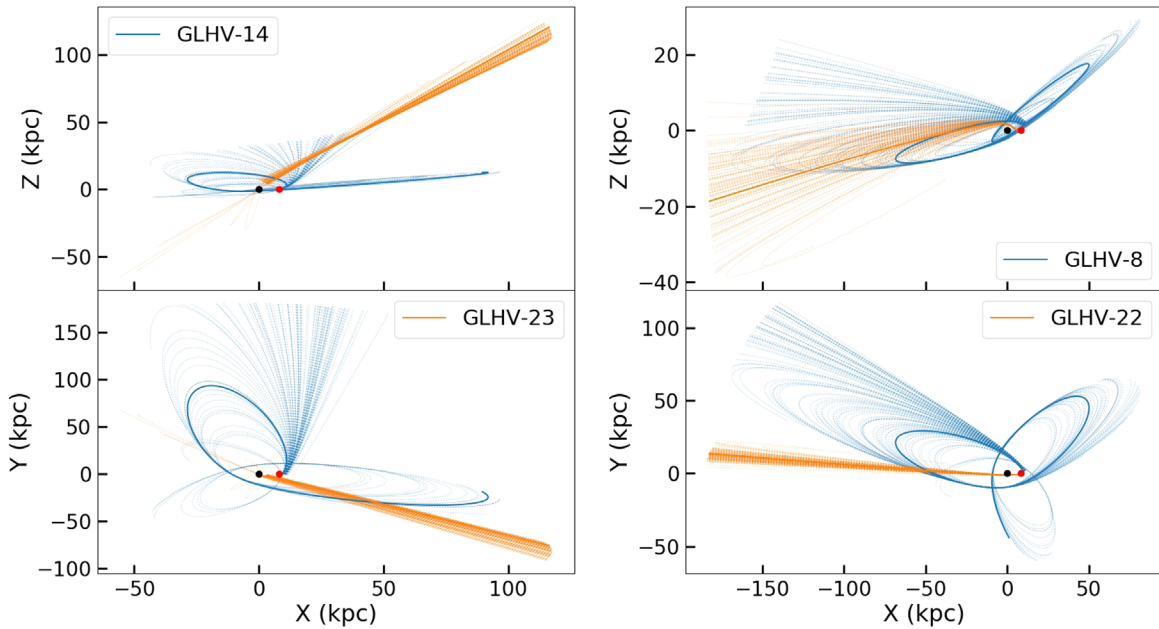
Figure 3. 2 Gyr backward orbit of the some represented HiVel stars in *XYZ* Galactocentric Coordinates. The red dot represents the Sun, and the black dot represents the GC. The thin lines show 100 orbits drawn at random from the uncertainties in the positions and velocities of each HiVel star, showing the uncertainty in the orbits.

Table 1
The Probability of Stars used as the Classified Criteria of HiVel Stars

Class	P_{gc}	P_{MW}	P_{ub}
HVS candidates	>0.16	⋯	⋯
OUT candidates	<0.16	>0.5	⋯
HRS candidates	<0.16	<0.5	>0.5
RS candidates	<0.16	<0.5	<0.5

those stars with $v_{\mathrm{gc}} > 0.85 v_{\mathrm{esc}}$, and derived a final sample of 24 HiVels with reliable astrometric parameters and RVs. We studied the metallicity and [α/Fe] distribution of our HiVel stars. Most of the HiVel stars are metal poor and α enhanced. Our results demonstrate that some HiVel stars could have originated from the GC or disk, while some from dwarf galaxies. To further understand the origin of HiVel stars, we traced the backward orbits of each star in the Galactic potential to derive probability parameters that are used to classify these HiVel stars. According to the classified criteria, 5 stars are from the tidal debris of accreted and disrupted dwarf galaxy, 19 stars are runaway stars candidates that originate from the disk of the Galaxy, and 6 of them are HRS candidates. There are two stars with high metallicity and low [α/Fe]. One of them is an "OUT" stars, which could have originated from the dwarf galaxy. The other is an "RS" star, which is similar to a thick disk star according to its orbit.

Appendix

Table 2 provides the positions and atmospheric parameters for 24 HiVel stars, and Table 3 provides the total velocities and distances and the probability of Stars used as the Classified Criteria of HiVel Stars.

Table 2
Atmospheric Parameters and Positions for 24 HiVel Stars, Classified into Three Subclasses

Notation	Source-id	R.A. (deg)	decl. (deg)	$T_{\rm eff}$ (K)	log(g) (dex)	[Fe/H] (dex)	[α/Fe] (dex)
OUT Candidates							
GLHV-9	4554190291969378048	263.38934	20.32675	4502	0.95	−2.12 ± 0.02	⋯
GLHV-14	1002667880552099328	106.79127	59.57526	5309	3.81	−0.07 ± 0.03	0.05 ± 0.1
GLHV-19	3905884598043829504	181.25391	9.45570	5062	2.47	−1.59 ± 0.01	0.22 ± 0.03
GLHV-20	4586965565362654464	278.93102	27.96378	4437	0.78	−2.07 ± 0.07	0.29 ± 0.04
GLHV-23	4450458649852400640	242.69749	7.16000	4752	1.70	−1.6 ± 0.02	0.26 ± 0.03
HRS Candidates							
GLHV-12	4443717204762199552	256.21663	9.35535	4389	1.26	−1.02 ± 0.04	0.17 ± 0.03
GLHV-13	4015088951907615744	185.47443	31.07946	5765	3.39	−1.02 ± 0.02	0.22 ± 0.03
GLHV-16	4491237203962217088	259.88425	8.67324	4710	1.53	−1.75 ± 0.03	⋯
GLHV-21	4443836776652403072	257.86499	10.21303	4469	1.31	−1.19 ± 0.03	0.24 ± 0.03
GLHV-22	2629296824480015744	335.83338	−2.51967	5212	3.18	−1.02 ± 0.01	0.19 ± 0.04
GLHV-24	1383279090527227264	240.33735	41.16677	4803	1.89	−1.4 ± 0.02	0.28 ± 0.03
RS Candidates							
GLHV-1	2503491051919554304	39.87357	3.10509	6236	4.16	−1.37 ± 0.02	0.47 ± 0.09
GLHV-2	1203885900077833984	237.11051	19.28888	4533	1.04	−2.21 ± 0.02	0.26 ± 0.03
GLHV-3	4485842140925368832	265.28990	6.23972	4149	0.62	−1.21 ± 0.05	⋯
GLHV-4	2106519830479009920	285.48442	45.97166	4468	1.33	−1.15 ± 0.02	0.2 ± 0.03
GLHV-5	1268023196461923712	225.78358	26.24632	4925	2.13	−1.53 ± 0.01	0.22 ± 0.03
GLHV-6	3784964943489710592	169.35630	−5.81368	4851	2.08	−1.14 ± 0.09	⋯
GLHV-7	1597988246569491968	233.62013	54.30564	5448	2.82	−1.05 ± 0.04	0.25 ± 0.04
GLHV-8	598766750854551168	131.80999	11.03167	6311	4.18	−0.24 ± 0.01	0.06 ± 0.1
GLHV-10	1255095276181144320	218.71274	25.16609	5439	4.50	−1.24 ± 0.05	0.32 ± 0.09
GLHV-11	330414789019026944	29.21933	36.66581	4976	2.15	−2.03 ± 0.01	0.19 ± 0.03
GLHV-15	1341901032000157056	258.13448	40.47352	4660	1.40	−2.04 ± 0.05	⋯
GLHV-17	1552278116525348096	204.66905	48.15653	5691	3.88	−0.85 ± 0.02	0.14 ± 0.1
GLHV-18	3736372993468775424	197.96401	11.28944	4946	2.21	−1.38 ± 0.04	0.21 ± 0.03

Table 3
Velocities and Distances for 24 HiVel Stars, Classified into Three Subclasses

Notation	rv_L (km s^{-1})	rv_G (km s^{-1})	$\overline{rv}$ (km s^{-1})	d (kpc)	$r_{\rm gc}$ (kpc)	$v_{\rm gc}$ (km s^{-1})	$P_{\rm MW}$	$P_{\rm ub}$
OUT Candidates								
GLHV-9	−315 ± 6	−319 ± 1	−319 ± 1	$10.3^{+2.0}_{-1.9}$	$7.9^{+1.3}_{-1.0}$	554^{+134}_{-124}	0.42	0.58
GLHV-14	−65 ± 4	−64 ± 1	−64 ± 1	$2.1^{+0.8}_{-0.6}$	$10.1^{+0.7}_{-0.5}$	583^{+129}_{-93}	0.21	0.79
GLHV-19	148 ± 5	149 ± 1	149 ± 1	$2.5^{+0.2}_{-0.2}$	$8.6^{+0.1}_{-0.1}$	519^{+69}_{-61}	0.48	0.52
GLHV-20	−238 ± 10	−234 ± 4	−235 ± 4	$10.5^{+1.6}_{-1.4}$	$9.3^{+1.1}_{-0.9}$	547^{+93}_{-85}	0.36	0.64
GLHV-23	−120 ± 6	−120 ± 1	−120 ± 1	$7.5^{+1.8}_{-1.2}$	$5.8^{+0.7}_{-0.2}$	711^{+194}_{-127}	0.08	0.92
HRS Candidates								
GLHV-12	−276 ± 4	−277 ± 0	−277 ± 0	$7.2^{+1.6}_{-1.1}$	$5.3^{+0.5}_{-0.1}$	593^{+163}_{-102}	1.00	0.62
GLHV-13	−56 ± 8	−55 ± 1	−55 ± 1	$2.1^{+0.4}_{-0.3}$	$8.7^{+0.1}_{-0.1}$	516^{+99}_{-72}	0.60	0.50
GLHV-16	−302 ± 6	−296 ± 2	−297 ± 1	$7.0^{+1.5}_{-1.2}$	$5.1^{+0.3}_{-0.1}$	603^{+149}_{-115}	1.00	0.63
GLHV-21	−184 ± 4	−182 ± 1	−183 ± 1	$13.0^{+2.8}_{-2.1}$	$8.5^{+2.3}_{-1.5}$	619^{+120}_{-90}	1.00	0.84
GLHV-22	−215 ± 5	−220 ± 4	−218 ± 3	$0.9^{+0.0}_{-0.0}$	$8.0^{+0.0}_{-0.0}$	568^{+22}_{-22}	1.00	0.98
GLHV-24	−179 ± 5	−181 ± 2	−181 ± 2	$6.2^{+0.7}_{-0.5}$	$8.8^{+0.3}_{-0.3}$	629^{+88}_{-66}	1.00	0.96
RS Candidates								
GLHV-1	361 ± 10	363 ± 1	363 ± 1	$0.4^{+0.0}_{-0.0}$	$8.5^{+0.0}_{-0.0}$	444^{+4}_{-4}	1.00	0.00
GLHV-2	−255 ± 6	−246 ± 2	−246 ± 2	$7.6^{+1.4}_{-1.3}$	$7.4^{+0.7}_{-0.4}$	479^{+42}_{-37}	0.81	0.19
GLHV-3	−17 ± 4	−8 ± 1	−8 ± 1	$6.9^{+2.3}_{-1.3}$	$4.9^{+0.5}_{-0.1}$	563^{+129}_{-76}	1.00	0.48
GLHV-4	−215 ± 4	−213 ± 1	−213 ± 1	$6.4^{+0.8}_{-0.6}$	$9.2^{+0.4}_{-0.3}$	457^{+51}_{-38}	1.00	0.17
GLHV-5	−275 ± 5	−277 ± 2	−277 ± 2	$3.9^{+0.4}_{-0.3}$	$7.6^{+0.0}_{-0.0}$	474^{+56}_{-42}	1.00	0.18
GLHV-6	128 ± 7	126 ± 1	126 ± 1	$3.3^{+0.5}_{-0.3}$	$9.0^{+0.2}_{-0.1}$	457^{+55}_{-36}	0.97	0.18
GLHV-7	41 ± 8	40 ± 1	40 ± 1	$1.2^{+0.1}_{-0.0}$	$8.2^{+0.0}_{-0.0}$	464^{+23}_{-20}	1.00	0.01
GLHV-8	75 ± 5	72 ± 2	72 ± 2	$3.2^{+0.7}_{-0.5}$	$10.7^{+0.6}_{-0.4}$	479^{+64}_{-48}	0.61	0.39
GLHV-10	367 ± 8	367 ± 2	367 ± 1	$0.2^{+0.0}_{-0.0}$	$8.1^{+0.0}_{-0.0}$	470^{+1}_{-1}	1.00	0.00
GLHV-11	−127 ± 5	−121 ± 2	−122 ± 2	$1.9^{+0.2}_{-0.1}$	$9.6^{+0.1}_{-0.1}$	491^{+48}_{-41}	1.00	0.37
GLHV-15	−219 ± 11	−222 ± 2	−222 ± 2	$6.1^{+0.9}_{-0.6}$	$8.4^{+0.4}_{-0.2}$	509^{+88}_{-60}	1.00	0.47
GLHV-17	−85 ± 6	−84 ± 2	−84 ± 2	$2.1^{+0.2}_{-0.1}$	$8.6^{+0.1}_{-0.0}$	490^{+53}_{-38}	1.00	0.31
GLHV-18	380 ± 7	378 ± 1	378 ± 1	$3.2^{+0.3}_{-0.3}$	$8.1^{+0.1}_{-0.0}$	499^{+21}_{-15}	1.00	0.18

ORCID iDs

Cuihua Du ⓘ https://orcid.org/0000-0002-3954-617X
Heidi Jo Newberg ⓘ https://orcid.org/0000-0001-8348-0983
Jianrong Shi ⓘ https://orcid.org/0000-0002-0349-7839
Jun Ma ⓘ https://orcid.org/0000-0001-6329-6644

References

Abadi, M. G., Navarro, J. F., & Steinmetz, M. 2009, ApJL, 691, L63
Bailer-Jones, C. A. L., Rybizki, J., Fouesneau, M., et al. 2018, AJ, 156, 58
Blaauw, A. 1961, BAN, 15, 265
Bland-Hawthorn, J., & Gerhard, O. 2016, ARA&A, 54, 529
Bromley, B. C., Kenyon, S. J., Brown, W. R., & Geller, M. J. 2009, ApJ, 706, 925
Bromley, B. C., Kenyon, S. J., Brown, W. R., & Geller, M. J 2018, ApJ, 868, 25
Brown, W. R., Geller, M. J., & Kenyon, S. J. 2009, ApJ, 690, 1639
Brown, W. R., Geller, M. J., & Kenyon, S. J. 2012, ApJ, 751, 55
Brown, W. R., Geller, M. J., & Kenyon, S. J. 2014, ApJ, 787, 89
Brown, W. R., Geller, M. J., Kenyon, S. J., & Kurtz, M. J. 2005, ApJL, 622, L33
Brown, W. R., Geller, M. J., Kenyon, S. J., & Kurtz, M. J. 2006, ApJ, 647, 303
Capuzzo-Dolcetta, R., & Fragione, G. 2015, MNRAS, 454, 2677
Cui, X. Q., Zhao, Y. H., Chu, Y. Q., et al. 2012, RAA, 12, 1197
Deng, L. C., Newberg, H. J., Liu, C., et al. 2012, RAA, 12, 735
Du, C. H., Li, H. F., Liu, S., Donlon, T., & Newberg, H. J. 2018, ApJ, 863, 87
Fragione, G., & Capuzzo-Dolcetta, R. 2016, MNRAS, 458, 2596
Gaia Collaboration, Brown, A. G. A., Vallenari, A., et al. 2016a, A&A, 595, A2
Gaia Collaboration, Brown, A. G. A., Vallenari, A., et al. 2018, A&A, 616, 1
Gaia Collaboration, Prusti, T., de Bruijne, J. H. J., et al. 2016b, A&A, 595, A1
Geier, S., Fürst, F., Ziegerer, E., et al. 2015, Sci, 347, 1126
Gvaramadze, V. V., Gualandris, A., & Portegies, Z. S. 2009, MNRAS, 396, 570
Hawkins, K., Kordopatis, G., Gilmore, G., et al. 2015, MNRAS, 447, 2046
Hills, J. G. 1988, Natur, 331, 687
Huang, Y., Liu, X.-W., Chen, B.-Q., et al. 2018, AJ, 156, 90
Huang, Y., Liu, X.-W., Zhang, H. W., et al. 2017, ApJ, 847, 9
Johnson, D. R. H., & Soderblom, D. R. 1987, AJ, 93, 864
Lee, D. M., Johnson, K. V., Sen, B., & Jessop, W. 2015, ApJ, 802, 48
Li, Y. B., Luo, A. L., Zhao, G., et al. 2012, ApJL, 744, L24
Li, Y. B., Luo, A. L., Zhao, G., et al. 2018, AJ, 156, 87
Lindegren, L., Hernández, J., Bombrun, A., et al. 2018, A&A, 616, A2
Luo, A. L., Zhao, Y. H., Zhao, G., et al. 2015, RAA, 15, 1095
Luri, X., Brown, A. G. A., Sarro, L. M., et al. 2018, A&A, 616, A9
Marchetti, T., Rossi, E. M., & Brown, A. G. A. 2018, 1804, arXiv:1804.10607v1
McMillan, P. J. 2017, MNRAS, 465, 76
Merritt, D. 2006, ApJ, 648, 976
Nissen, P. E., & Schuster, W. J. 2010, A&A, 511, L10
Perets, H. B., & Šubr, L. 2012, ApJ, 751, 133
Portegies, Zwart S. F. 2000, ApJ, 544, 437
Purcell, C. W., Bullock, J. S., & Kazantzidis, S. 2010, MNRAS, 404, 1711
Sesana, A., Haardt, F., & Madau, P. 2006, ApJ, 651, 392
Sesana, A., Haardt, F., & Madau, P. 2007, MNRAS, 379, L45
Tauris, T. M. 2015, MNRAS Lett., 448, L6
Teyssier, M., Johnston, K. V., & Shara, M. M. 2009, ApJL, 707, L22
Tian, H. J., Liu, C., Carlin, J. L., et al. 2015, ApJ, 809, 145
Wang, B., Justham, S., & Han, Z. 2013, A&A, 559, A94
Williams, A. A., Belokurov, V., Casey, A. R., & Evans, N. W. 2017, MNRAS, 468, 2359
Wu, Y., Luo, A.-L., Li, H.-N., et al. 2011, RAA, 11, 924
Xiang, M. S., Liu, X. W., Yuan, H. B., et al. 2015, MNRAS, 448, 822
Xiang, M. S., Liu, X. W., Yuan, H. B., et al. 2017, MNRAS, 467, 1890
Xu, Y., Newberg, H. J., Carlin, J. L., et al. 2015, ApJ, 801, 105
Yu, Q., & Tremaine, S. 2003, ApJ, 599, 1129
Zhang, Y. Q., Smith, M. C., & Carlin, J. L. 2016, ApJ, 832, 10
Zhao, G., Zhao, Y. H., Chu, Y. Q., et al. 2012, RAA, 12, 723
Zheng, Z., Carlin, J. L., Beers, T. C., et al. 2014, ApJL, 785, 23
Zhong, J., Chen, L., Liu, C., et al. 2014, ApJL, 789, L2